Comptes Rendus
Géoscience — Sciences de la Planète
Supplementary material to the article available at:
https://doi.org/10.5802/crgeos.251

Supplementary material: Fluvial terrace formation in mountainous areas: (1) Influence of climate changes during the last glacial cycle in Albania

Oswaldo Guzmán [a, b], Jean-Louis Mugnier [*, b], Riccardo Vassallo [b], Rexhep Koçi [c], Julien Carcaillet [b] and François Jouanne [b]

[a] Grupo de Investigación en Ciencias de La Tierra y Clima, Universidad Regional Amazónica Ikiam, Muyuna, Ecuador

[b] ISTerre, Université Grenoble Alpes, Université Savoie Mont Blanc, CNRS, IRD, Le Bourget du Lac, France

[c] Institute of Geosciences of the Polytechnical University of Tirana, Albania

E-mail: jemug@univ-smb.fr (J.-L. Mugnier)

Appendix 1. Technical details for ^{14}C dating and location of the samples

Method

The ^{14}C ages were calibrated using the OxCal program version 4.3 [Ramsey, 2009], based on the IntCal 13 dataset [Reimer et al., 2013]. The polynomial calibration of Bard et al. [2004] is also used to define an upper bound for the ages of the oldest samples (^{14}C ages > 45,300 yr BP) because the OxCal calibration does not define the upper bound in such cases. Calibrated ages are given as a time interval linked to the two sigma (95%) probability. Previously published ^{14}C ages [Lewin et al., 1991, Woodward et al., 2008, Carcaillet et al., 2009, Koçi et al., 2018] were re-calibrated following the same procedure (Table 3).

Location of samples for ^{14}C dating

The ^{14}C dating has been performed on organic matter (Figure S1a, Appendix 1), located in the lower part of the fine grain deposits (Figure S1a, Appendix 1, left part) or fine grain deposits interbedded with gravel deposits (Figure S1c, Appendix 1). For each sample, a simplified log of has been performed (Figure S1a, Appendix 1, right part). The location of the sample with respect to the surface is indicated in a column in Table 3.

* Corresponding author.

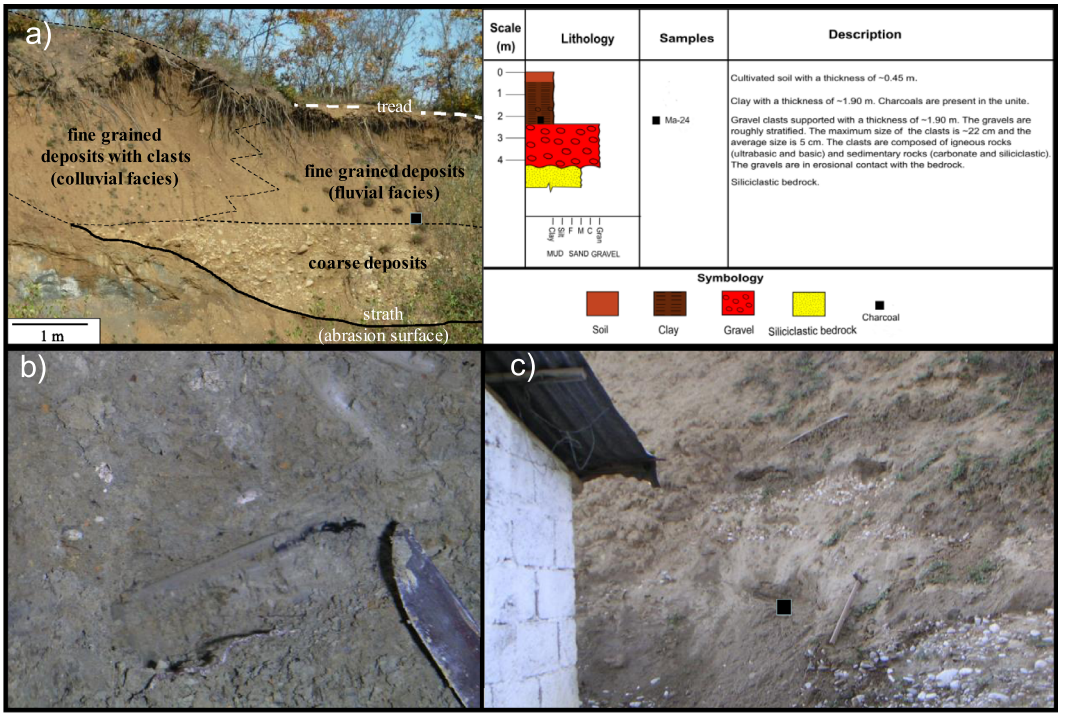

Supplementary Figure S1. Examples of charcoals found in the units; (a) photography (left) and lithological profile (right) (Sample Ma-24) of the Mat River (Terrace $T3_{(ma)}$); (b) Close photography of sample Ma-24; (c) photography of a site in a fill terrace ($T5_{(vj)}$).

Appendix 2. Technical details for ^{10}Be dating and description of the attenuation profiles

Method

Exposure ages [Lal, 1991, Brown et al., 1991] have been determined from the ^{10}Be concentration in siliceous rich pebbles collected along the depth profiles. This sampling strategy allowed to estimate the ^{10}Be inherited from prior exposure [Repka et al., 1997] and an analysis of the attenuation profiles with a Monte Carlo simulator [Hidy et al., 2010] can be used to estimate the surface erosion and the exposition age as well as their uncertainties. However, the low density of the sampling (4 to 5 samples in 3 to 6 m deep profiles) and the dispersion of the analytical results could make the erosion calculation imprecise. Therefore, we decided to only estimate a minimum age for the surface by assuming a null erosion rate.

When the outcrops cannot be used to make a profile or when boulders are not found at the surface, numerous (several tens) individual pebbles were taken from the surface of the terrace and analyzed as a single sample. This strategy makes it possible to homogenize the ^{10}Be concentrations in contexts where inheritance may induce a scattering of the surface concentrations although this strategy is only providing maximum ages, unless it can be shown that inheritance is negligible with respect to exposure time. The parameter values used to calculate the ^{10}Be ages are indicated in the following.

Beryllium were extracted following the chemical procedures of Brown et al. [1991] and Merchel and Herpers [1999]. The extractions were made at the GeoThermoChronology platform of ISTerre (France). ^{10}Be concentrations were measured at the accelerator mass spectrometry facility ASTER (CNRS, France) [Arnold et al., 2010]. They were calibrated against NIST Standard Reference Material 4325 using the assumed ^{10}Be/^{9}Be ratio of $2.79 \pm 0.03 \times 10^{-11}$, and a ^{10}Be half-life of 1.387 ± 0.012 Ma [Chmeleff et al., 2010, Korschinek et al., 2010]. Exposure ages were calculated using the online CREp calculator and the attenuation profiles with the software developed by Hidy et al., [2010].

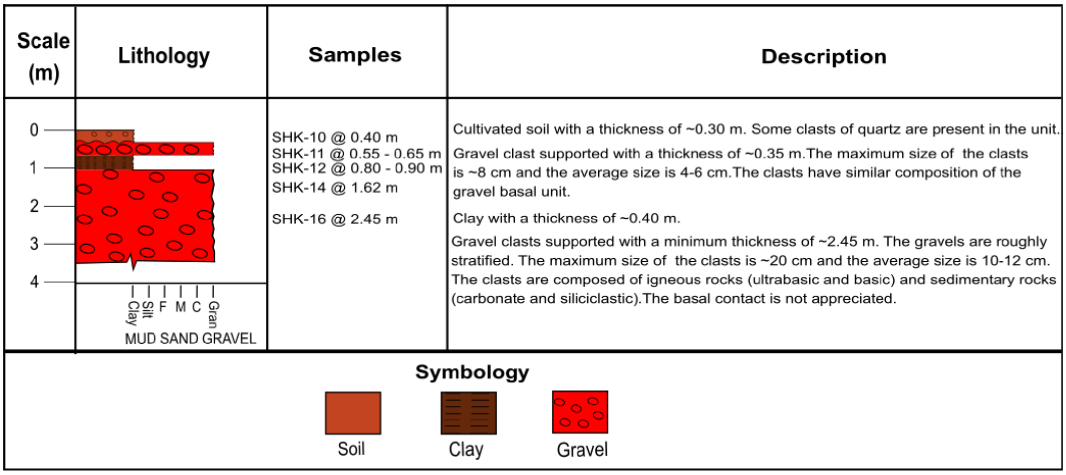

Supplementary Figure S2. Lithological description of the Shkumbin River ^{10}Be cosmogenic profile.

Production rates were calculated following Stone [2000] using the modified scaling functions of Lal [1991] and a ^{10}Be production rate in quartz of 4.09 ± 0.19 at·g^{-1}·yr^{-1} at sea level and high latitude [Martin et al., 2017]. Geomorphic shielding factors were calculated following Dunne et al. [1999]. All ^{10}Be age calculations were performed using attenuation lengths of 160, 1500, and 5300 g/cm^2 with associated relative contributions to the total production rate of 97.85%, 1.50%, and 0.65% for neutrons, slow muons, and fast muons, respectively [Braucher et al., 2003]. Density of 2.2 is used for recent sediment (less than 20 ka old) and 2.4 for older sediment (more than 100 ka old) to take into account the time dependent compaction of the sediment. A null correction for recurrent snow cover was assumed as the sites are close to the Adriatic Sea and their altitude is less than 500 m.

^{10}Be concentration uncertainties (Table 2) include analytical errors from the counting statistics and blank correction, whereas age uncertainties also include the errors of the production rate linked to the ^{10}Be decay constant [Chmeleff et al., 2010, Korschinek et al., 2010] and introduced by the scaling models of Lal [1991] and Stone [2000].

We measured the ^{10}Be attenuation (Table 1, main text) along two depth profiles (Shkumbin River and Ulza Dam in Mat River) and measured the ^{10}Be concentration in amalgamated clast samples located on two terrace tops (Ma-04 and Ma-06) (locations on Figure 1, main text; see the description in the following). Previously published ^{10}Be ages [Carcaillet et al., 2009] were re-calibrated following the same procedure (Table 2, main text).

Shkumbin (Paleo-Devoll) River ^{10}Be profile

In the lower reaches of the Paleo-Devoll catchment, a cosmogenic depth profile was made through the alluvial deposit of $T3_{(pa)}$ (Figure 6a, main text).

Each sample was formed by one cobble of siliceous rock (e.g. granite, quartzite) except Shk-12, which consisted of an amalgamation of small siliceous pebbles, collected in a depth interval of 10 cm. The sampled terrace is nowadays used for agriculture; thus, the upper 25 cm was assumed as the ploughing depth. The first sample (Shk-10 in Table 2) was taken at 30 cm below surface; this sample had a ^{10}Be concentration of $7.70 \pm 0.72 \times 10^4$ at/g. The ^{10}Be concentration of all the samples does not show a clear attenuation trend with depth. The unexpected high ^{10}Be concentration of sample Shk-16 may be explained by a provenance from a neighboring tributary stream shed creating a different pre-exposure history. Chemical problems during sample preparation could account for the low concentration measured for sample Shk-11. Three samples (Shk-10, 12, 14) nonetheless allow estimating an exponential theoretical evolution of production with depth. Assuming no denudation, assigning a material density of 2.2 g/cm^3 to the alluvial material, and using a chi-squared inversion to minimize the difference between observed and modeled ^{10}Be data, a maximum

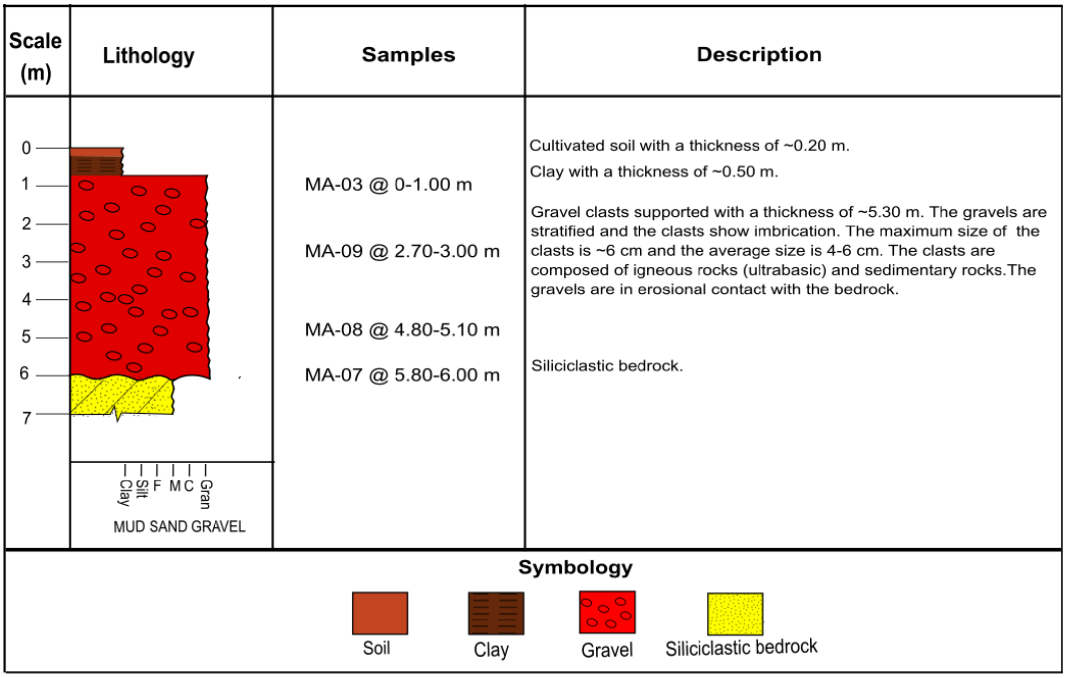

Supplementary Figure S3. Lithological description of the Mat River ^{10}Be cosmogenic profile.

inherited concentration of $4.03 \pm 0.32 \times 10^4$ at/g was estimated. These results yielded a minimum exposure age of 18.81 ± 2.4 ka (^{10}Be) for $T3_{(pa)}$.

Mat River ^{10}Be profile

In the middle reaches of the Mat River, a cosmogenic depth profile was made through the alluvial deposits of terrace $T8_{(ma)}$ close to the Ulza dam (Figure 6b, main text).

Each sample was formed by an amalgamation of small siliceous pebbles. The first sample (Ma-03 in Table 1, main text) was collected at a depth of 10 cm. This sample had a concentration of $4.40 \pm 0.14 \times 10^5$ at/g. Assuming no denudation, assigning a material density of 2.4 g/cm^3 to the alluvial material, and considering the concentration of the lower sample collected at 590 cm as the inherited ^{10}Be concentration ($0.26 \pm 0.01 \times 10^5$ at/g), this profile yielded a minimum exposure age of 100.8 ± 9.4 ka (^{10}Be).

Appendix 3. A synthesis of previous studies of the Vjosa terraces

For the Vjoja River, we combined several works [Lewin et al., 1991, Hamlin et al., 2000, Woodward et al., 2008, Guzmán et al., 2013, Hauer et al., 2021] and homogenized the nomenclature and labelled the terrace surfaces (normal characters in Table 3, main text) located at the top of the previously defined units (italic characters in Table 3, main text). The Vjoja River is more than 272 km long and is made up of four sections characterized by very different morphologies and hydrodynamics [Hauer et al., 2021]. In the upper section (Konista area of the Vjosa-Voidomatis River in Greece, Figure 1, main text), four sedimentary units (Kipi, Aristi, Vikos and Klithi units of Lewin et al. [1991] and Hamlin et al. [2000]) were initially described, whereas Woodward et al. [2008] identified seven units (*U8* to *U2*) in addition to the present-day channel (*U1*). *U8* was deposited by a fluvial system with a much more extensive catchment that drained areas where extensive ophiolite rocks cropped out, probably before 350 ka [Macklin et al., 1997]. Detailed sedimentology and lithological studies [Lewin et al., 1991] show that *U3* recorded a change in the sediment source linked to the glacier retreat at the end of the last cold stage. The units older than *U3* are mainly coarse-grained alluvial units [Woodward et al., 2001, 2008]. *U3* and *U4* locally contain fine-grained slackwater sediments that had been extensively studied to determine the

Supplementary Table S1. Correlation of the local terrace nomenclatures of the Vjoja River with the regional nomenclature for the Albanian terraces

River	Middle section		Vjosa upper section		Regional nomenclature	Regional abandonment ages (ka)
Author	*Prifti and Meçaj (1987)*	*Guzman et al. (2013)*	*Woodward et al., 2008*	This study		
T	T_V *(P & M)*		*U8*	$T10_{(vj)}$	**T12**	**>350 ?**
e				T9(vj)	**T11**	**>193**
r					**$U10_{(pa)}$**	
r	T_{IV} *(P & M)*		*U7*	$T8_{(vj)}$	**T10**	**90-117**
a	T_{III} *(P& M)*		*U6*	$T7_{(vj)}$	**T9**	**68-87**
c	T_{II} *(P & M)*		*U5*	$T6_{(vj)}$	**T8**	**52 (-2/+3)**
e				-	**T7**	**42 (-0.5/+1.5)**
				-	**T6**	**35.5 (-1/+2)**
	T_I *(P & M)*			$T5_{(vj)}$	**T5**	**29.5 (± 1)**
			U4	$T4_{(vj)}$	**T4**	**25 (-2/+1)**
			U3	$T3_{(vj)}$	**T3**	**16.5-22**
				-	**T2**	**11-12**
		T_1 *(G & al.)*	*U2*	T2(vj)	**T1**	**5.7-6.3; 7.6-10**
			U1-actual	$T1_{(vj)}$	**T0**	**0.2-1**
					T0	**0-0.2**

The light green and light red cells refer to dated and poorly correlated levels, respectively. The colored cells on the right side refer to the color code of Figures 4, 5, 8, 9 and 10 main text. The regional ages of the terrace abandonment (last column) are obtained from the probability density curves of the numerical dating for terraces younger than 60 ka (see main text and Appendix 6).

evolution of the glacier: Slackwater sediments were deposited by a series of large floods in a river system fed by meltwaters from glaciers sometime after 21.3 ka [Hamelin, 2000, Woodward et al., 2001], whereas they were deposited close to 17.9–16.2 cal ka by a series of rainfall-generated floods that exclude the glacial activity at that time [Woodward et al., 2008]. Seven units were dated using different methods [^{14}C, U/Th, ESR, TL; Woodward et al., 2001, 2008]. The numeric ages, except for *U4*, come from the upper part of the sedimentary units and therefore are considered close to the age of abandon. Amongst these data (Table 2), two TL ages have been removed from the following analysis: The >150 ka age of the VOI26 sample [Lewin et al., 1991] provides a lower bound for the age of *U8* that is not meaningful as it is much younger that the age (>350 ka) inferred from the lithology and provenance criteria [Macklin et al., 1997]. Sample VOI23 provides an age of 20.2 ± 7 ky [Lewin et al., 1991] and its large uncertainty makes this age questionable, especially since there is a temporal discrepancy between the gravels of unit *U6*, dated at 80 ± 7 and 74 ± 6 ky; furthermore, the fine-grained pedogenic deposits of sample VOI23 has been interpreted as a later deposition associated with eolian processes [Woodward et al., 2008].

Taking the geometries described by Lewin et al. [1991], Woodward et al. [2001] and Woodward et al. [2008] into account, it has been found that the *U8* and *U7* units are related to fill terraces that are at least 23 and 26 m thick, respectively; the substratum riser between these two units is generally hidden. The top of *U6*, *U5* and *U4* are respectively 12.7, 10 and 9.3 m above the channel bed close to the old Klithonia bridge [Woodward et al., 2008]. The substratum riser does not outcrop between these terraces and *U6*, *U5* and *U4* are probably fill terraces or thick fill-cut terraces formed during a slow process of downcutting within the *U7* fill terrace. *U3* is a thin fill-cut terrace at the Klithonia bridge [Lewin et al. 1991] and is superposed onto unit *U4* at the Boila rock shelter [Woodward et al. 2001]. Lastly, *U2* is a Holocene fill

terrace. The incision rate is greater in the middle section of the Vjosa River than in the upper section [Guzman et al., 2013]. The elevation of the highest terrace reaches at least 160 m [Prifti, 1981] and substratum risers frequently outcrop between the nested fill terraces. Prifti and Meçaj [1987] mapped five nested fill terrace levels (T_I *to* T_V in Table 3, main text) whereas Guzman et al. [2013] mapped another terrace level [T1 of Guzman et al., 2013], encased within the T_I terrace of Prifti and Meçaj [1987], and located at the top of a valley fill; this valley fill extends several tens of meters below the present river, according to geophysical data [Prifti, 1981]. The highest level T_V is more than 70 m thick and the lithology of T_V is slightly different from that of the other terraces with 15%–25% igneous rocks debris, 35%–45% sand derived from flysch deposits, 35%–40% from carbonate debris whereas the other terraces contain very few igneous rocks [Prifti, 1981]. Therefore, T_V can be correlated with unit *U8* of Woodward et al. (2008) and is probably >350 ka old. Our field work has shown that the surface of T_V is complex, with hills locally formed by a conglomerate unit preserved between meanders of a terrace cut within T_V. The conglomeratic units beneath the terraces are mainly formed of rounded fluvial clasts. Nonetheless, angular calcareous clasts are intercalated in numerous places within the fluvial sediments. They are related to debris flows provided from very steep calcareous slopes, such as the one illustrated on Figure 2b, main text. Guzman et al. [2013] dated the T_I terrace at 27.78–28.84 cal kyr BP (Table 2, main text). Therefore, the age of T_I is intercalated between the ages of Units *U4* and *U5* provided by Woodward et al. [2008]. Guzman et al. [2013] estimated the top of the valley fill T_1 to be ≥4.09–4.43 cal kyr BP based on colluvium dating. The other ages of the terraces, presented by Hauer et al. [2021] and initially proposed by Koçi [2014], are the results of only a very preliminary correlation that is revised in this paper (Sections 5.2 and 5.3).

Hence, when the studies of the upper and middle sections of the Vjosa River are considered, ten river terrace levels are identified $T10_{(vj)}$ to $T1_{(vj)}$, from oldest to youngest (see Table S1, Appendix 3 for the correspondence with the works of Pfifti and Meçaj [1987] and Woodward et al. [2008]) and nine are dated using different methods (see above). The ages of $T10_{(vj)}$, $T8_{(vj)}$, $T7_{(vj)}$, $T6_{(vj)}$, $T5_{(vj)}$, $T4_{(vj)}$, $T3_{(vj)}$, $T2_{(vj)}$, and $T1_{(vj)}$ are: >350 ka, 113 ± 6.00 ka, 68.00–87.00 ka, 49.00–61.50 ka, 27.78–28.84 cal kyr BP, 21.70–27.90 ka, 16.20–23.75 ka, >4.09–4.43 cal yr BP, and 0.56–1.05 cal yr BP, respectively (Figure 3a, Main text) and $T9_{(vj)}$ is not dated.

Appendix 4. Paleo current data from the Gostimë-Cërrik plain

The rose diagrams with the results are represented in Figure 4c, main text.

Site	Azimuth	Dip	Sedimentary structure
Gostimë 40°59′33″N 20°00′32″E	25	40 SE	Imbricated clast
	20	30 SE	Imbricated clast
	25	50 SE	Imbricated clast
	32	45 SE	Imbricated clast
	29	30 SE	Imbricated clast
	40	40 SE	Imbricated clast
	5	40 SE	Imbricated clast
	25	20 SE	Imbricated clast
	27	25 N	Imbricated clast
	30	10 SE	Imbricated clast
	10	30 SE	Imbricated clast
	300	12 W	Cross stratification
Cërrik 41°01′39″N 19°58′54″E	10	45 E	Imbricated clast
	60	25 SE	Imbricated clast
	50	45 SE	Imbricated clast
	67	25 SE	Imbricated clast
	70	30 E	Imbricated clast
	15	25 E	Imbricated clast
	60	40 SE	Imbricated clast
	65	30 SE	Imbricated clast
	60	35 SE	Imbricated clast
	65	30 SE	Imbricated clast
	74	30 E	Imbricated clast
	68	22 E	Imbricated clast
	6	20 E	Imbricated clast
	60	40 SE	Imbricated clast
	15	1E	Imbricated clast
	75	15 E	Imbricated clast
	65	30 SE	Imbricated clast
	70	25 SE	Imbricated clast
	50	25 SE	Imbricated clast
	25	25 SE	Imbricated clast
	45	40 SE	Imbricated clast
	70	55 SE	Imbricated clast

Appendix 5. Geomorphologic maps of the paleo-Devoll River

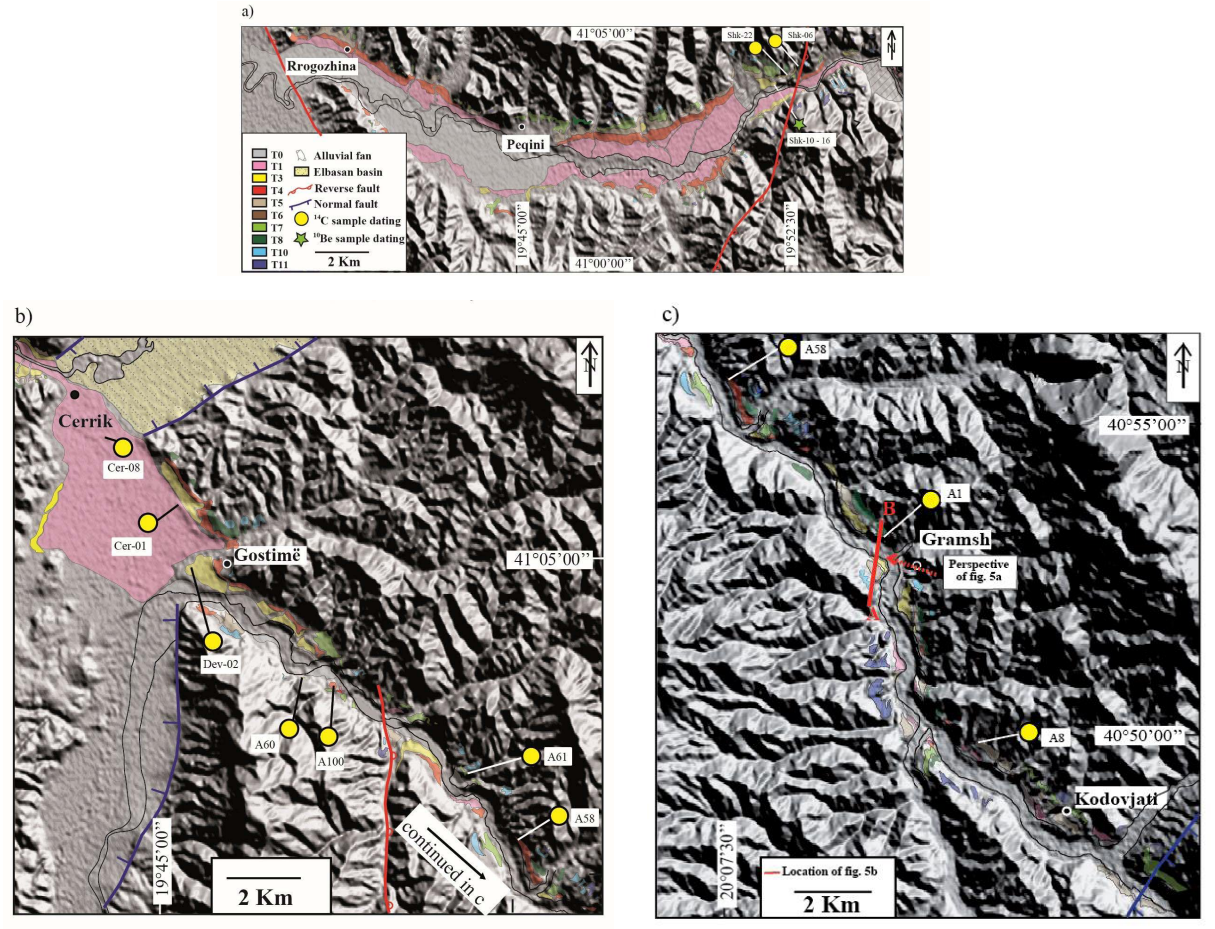

Supplementary Figure S4. Locations of a, b and c are shown in Figure 1, main text. (a) Lower reaches of the paleo-Devoll (present-day Shkumbin River). (b) The Cërrik plain and middle reaches of the paleo-Devoll River. (c) Upper reaches of the paleo-Devoll River.

Appendix 6. Determination of regional terrace levels from a time correlation

Thirty-one out of the 49 local terrace levels ($Tx_{(river)}$, Figure 3, main text) recognized along the seven rivers were dated, providing a solid framework for a regional correlation (Tx) based on the synchronicity of numerical ages. To take into account the uncertainties of the 60 numerical ages younger than 60 ka, the individual probability distribution ages were summed and a regional probability density curve [Ramsey, 2009] was obtained. This method was already used in terrace chronology studies [e.g. Meyer et al., 1995, Wegmann and Pazzaglia, 2002, 2009]. The summation (Figure S5, Appendix 6) shows zones, where the probability of sedimentation is null, that separate ten high probability peaks and that define the ages of T0 to T8.

The peak ages younger than 2 ka (gray color on Figure S5, Appendix 6) refer to the morphological flood plain T0. The T0-level ages are dispersed between less than 0.2 ka and 2 ka. This dispersion highlights that the development of this recent terrace level is not instantaneous but extends a few thousand

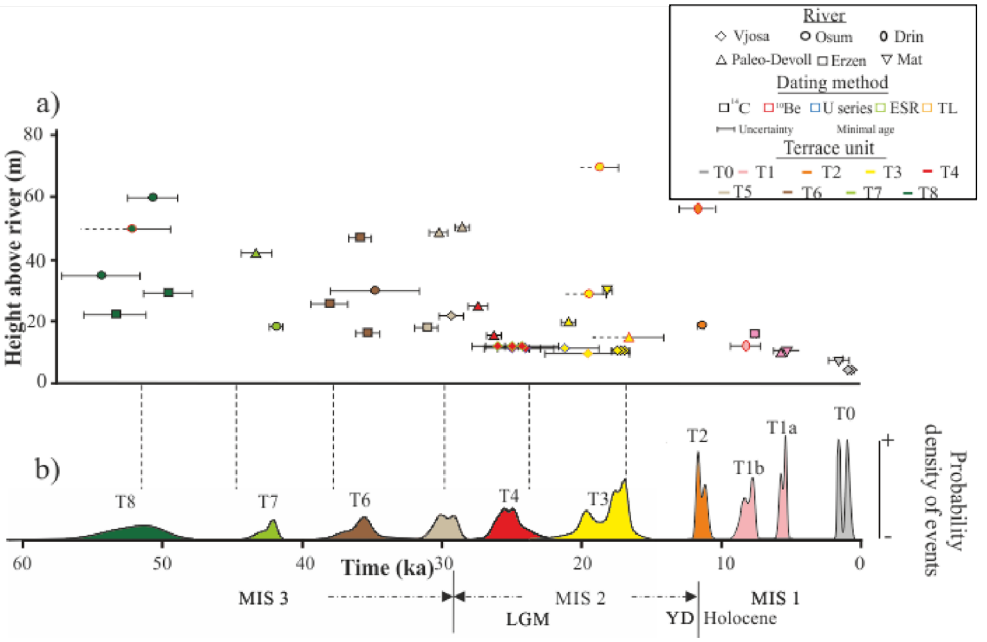

Supplementary Figure S5. Compilation of the Albanian terrace ages for the last 60 ka (Table 3, main text). (a) Plot of individual ages and their two sigma (95%) probability. Each terrace is represented by a symbol related to the river, the contour color and the fill color correspond to the dating method and the terrace level (regional nomenclature), respectively. The horizontal axis corresponds to the terrace age while the vertical axis represents the height of the terrace above the present-day river. (b) The regional probability density curve produced by summing the probability distribution of the individual ages. MIS, LGM and YD stand for Marine Isotope Stage [Shackleton, 1987], Last Glacial Maximum [Clark et al., 2009] and Younger Dryas [Berger, 1990], respectively.

years depending on the distribution of the extreme flooding events and this time-scale could probably be inferred for any terrace level development. Furthermore, two encased terraces of the Erzen River ($T1_{(er)}$ and $T2_{(er)}$) are younger than 2 ka, showing that recent temporal fluctuations in flood intensity can lead to complex morphological floodplain geometries.

Holocene ages have been grouped together in a T1 regional level (pink color on Figure S5, Appendix 6). Ages between 7.6 and 10 ka have been found for the terraces $T3_{(er)}$ developed at the wind gap between the Erzen and Tirana rivers and to $T2_{(dr)}$. Ages close to 5.7–6.3 ka are related to the terrace level $T2_{(pa)}$ developed at the wind gap between the Devoll and Shkumbin rivers (Figure 4, main text) and to $T2_{(ma)}$.

Ages close to 11 ka have been grouped together in a T2 regional level (sand-yellow color on Figure S5, Appendix 6). They are found along the Drin [Gemignani et al., 2022] and Osum [Carcaillet et al., 2009] rivers.

The probability density curve between 21 and 16.6 ka, although formed of several peaks, is continuous (yellow color on Figure S5, Appendix 6) and groups together the ages found for $T3_{(Vj)}$, $T3_{(os)}$, and $T3_{(pa)}$. We considered that this large distribution refers to a regional level T3 abandoned at the end of the Last Glacial Maximum (LGM).

The sharp peak of the probability density curve (red color on Figure S5, Appendix 6) found at 25 (−2/+1) ka groups together the ages of $T4_{(Vj)}$ and $T4_{(pa)}$. Similarly, the four (light brown, dark brown, light green and dark green color peaks on Figure S5, Appendix 6, respectively) found at 39 (±1), 35.5 (−1/+2), 42 (−0.5/+1.5) and 52 (−2/+3) ka correlate the terraces dated on the different rivers (light green

levels in Table 3, main text). They define the regional levels T5 to T8, respectively.

The ages greater than 60 ka are few in number. The T9 regional level (orange color on Figure 3, main text) is only defined from the $T7_{(vj)}$ dating, with an age of 68 to 87 ka. The T10 regional level (light blue color on Figure 3, main text) is defined from the upper Vjosa River ($T8_{(vj)}$) and the Mat River ($T8_{(ma)}$) with an age of 90 to 117 ka. The T11 level (navy blue on Figure 3, main text) is only defined from $T9_{(ma)}$, dated at $>202 \pm 20$ ka. The age of the oldest T12 (purple-blue on Figure 3, main text) is only estimated from $T10_{(vj)} > 350$ ka [Woodward et al., 2008].

Along the various rivers, eighteen recognized terrace levels are not numerically dated, and their elevation relative to the dated terrace levels only provides a poor relative chronology. The intercalation of $T6_{(pa)}$ level between two dated terraces would nonetheless suggest that it correlates with the regional level T6 and the similitude of the superposition relationships between the $T4_{(os)}/U5_{(os)}$ and $T5_{(pa)}/U6_{(pa)}$ pairs would suggest that $T4_{(os)}$ correlates with T5 (light yellow cells in Table 3, main text). Finally, $T1_{(os)}$, $T1_{(pa)}$ and $T1_{(dr)}$ form the morphological flood plains [Hauer et al., 2021] and therefore correlate with T0.

References

Arnold, M., Merchel, S., Bourles, D., Braucher, R., Benedetti, L., Finkel, R. C., Aumaitre, G., Gottdang, A., and Klein, M. (2010). The French accelerator mass spectrometry facility ASTER: Improved performance and developments. *Nucl. Instrum. Methods Phys. Res. B*, 268, 1954–1959. https://www.sciencedirect.com/science/article/abs/pii/S0168583X10002028.

Braucher, R., Brown, E. T., Bourlès, D. L., and Colin, F. (2003). *In situ* produced ^{10}Be measurements at great depths: implications for production rates by fast muons. *Earth Planet. Sci. Lett.*, 211, 251–258.

Brown, E. T., Edmond, J. M., Raisbeck, G. M., Yiou, F., Kurtz, M. D., and Brook, E. J. (1991). Examination of surface exposure ages of moraines in Arena Valley, Antarctica, using *in situ* produced ^{10}Be and ^{26}Al. *Geochim. Cosmochim. Acta*, 55, 2269–2283.

Chmeleff, J., Von Blanckenburg, F., Kossert, K., and Jakob, D. (2010). Determination of the ^{10}Be half-life by multicollector ICP-MS and liquid scintillation counting. *Nucl. Instrum. Methods Phys. Res.*, 268, 192–199. https://www.sciencedirect.com/science/article/abs/pii/S0168583X09009793?via%3Dihub.

Dunne, J., Elmore, D., and Muzikar, P. (1999). Scaling factors for the rates of production of cosmogenic nuclides for geometric shielding and attenuation at depth on sloped surfaces. *Geomorphology*, 27, 3–11. https://www.sciencedirect.com/science/article/abs/pii/S0169555X98000865.

Korschinek, G., Bergmaier, A., Faesterman, T., Gerstmann, U. C., Knie, K., Rugel, G., Wallner, A., Dillmann, I., Dollinger, G., Lierse von Gostomski, C., Kossert, K., Maiti, M., Poutivsev, M., and Remmert, A. (2010). A new value for the half-life of ^{10}Be by heavy-Ion elastic recoil detection and liquid scintillation counting. *Nucl. Instrum. Methods Phys. Res. B*, 268, 187–191.

Lal, D. (1991). Cosmic ray labeling of erosion surfaces: *In situ* nuclide production rates and erosion models. *Earth Planet. Sci. Lett.*, 104, 424–439.

Martin, L. C. P., Blard, P.-H., Balco, G., Lavé, J., Delunel, R., Lifton, N., and Laurent, V. (2017). The CREp program and the ICE-D production rate calibration database: a fully parameterizable and updated online tool to compute cosmic-ray exposure ages. *Quat. Geochronol.*, 38, 25–49.

Merchel, S. and Herpers, U. (1999). An update on radiochemical separation techniques for the determination of long-lived radionuclides via accelerator mass spectrometry. *Radiochim. Acta*, 84, 215–219.

Reimer, P. J., Bard, E., Bayliss, A., Beck, J. W., Blackwell, P. G., Bronk Ramsey, C., Grootes, P. M., Guilderson, T. P., Haflidason, H., Hajdas, I., Hatté, C., Heaton, T. J., Hoffmann, D. L., Hogg, A. G., Hughen, K. A., Kaiser, K. F., Kromer, B., Manning, S. W., Niu, M., Reimer, R. W., Richards, D. A., Scott, E. M., Southon, J. R., Staff, R. A., Turney, C. S. M., and van der Plicht, J. (2013). IntCal13 and Marine13 radiocarbon age calibration curves 0–50,000 years cal BP. *Radiocarbon*, 55, 1869–1887.

Repka, J. L., Anderson, R. S., and Finkel, R. C. (1997). Cosmogenic dating of fluvial terraces, Fremont River, Utah. *Earth Planet. Sci. Lett.*, 152, 59–73.

Stone, J. O. (2000). Air pressure and cosmogenic isotope production. *J. Geophys. Res.*, 105(B10), 753–759.